Supplementary Materials

Heat Transport Architecture Governs the Performance of Large-Area Flexible Thermoelectric Cooling

Jun Pei[a,†,*], Jiazhang Li[b,†], Hao Rao[c], Chun-Yu Li[a], Xianxin Zhang[a], Dai-Bing Zhang[d], Wei Gao[a], Hezhang Li[e,*]

[a] The Beijing Municipal Key Laboratory of New Energy Materials and Technologies, School of Materials Science and Engineering, University of Science and Technology Beijing, Beijing, 100083, China;
[b] School of Science, Beijing University of Posts and Telecommunications, Beijing, 100876, China;
[c] China Star Network, Network Application Research Institute Co., Ltd., Beijing, 100160, China;
[d] Inner Mongolia Key Lab Nanoscience & Nanotechnology, School of Physical Science and Technology, Inner Mongolia University, Hohhot 010021, China;
[e] Department of Precision Instrument, Tsinghua University, Beijing, 100084, China

†Jun Pei and Jiazhang Li contributed equally to this work as the first authors.
*Corresponding author: Jun Pei (junpei@ustb.edu.cn); Hezhang Li (lihezhang1202@mail.tsinghua.edu.cn);

Supplementary Note S1: Hydraulic analysis and practical operating envelope

The pressure drop along the flow channels was estimated with the Darcy–Weisbach equation, $\Delta p = f\,(L/D_h)(\rho u^2/2)$, with the Darcy friction factor f taken from the laminar or turbulent correlation appropriate to the Reynolds number $R_e = \rho u D_h/\mu$, where u is the mean velocity, D_h the hydraulic diameter, ρ the density and μ the dynamic viscosity. The required pumping or fan power follows from $P = Q\Delta p/\eta$, with Q the volumetric flow rate and η the pump/fan efficiency (taken as η: 0.70). For the water-cooled blanket (L = 2.0 m, D_h = 8 mm), the reported velocity of 152.79 m/s corresponds to $R_e \approx 1.37\times10^6$ and $\Delta p \approx 34912$ kPa, giving P ≈ 383039 W; for the air-cooled blanket (D_h = 250 mm) the corresponding values are Re ≈ 2.44×10^6, Δp ≈ 1216 Pa and P ≈ 13030 W. On this basis a practical operating envelope of u ≤ 6 m/s (Re ≤ 5.4×10^4) and Δp ≤ 90 kPa is adopted in the discussion, and the extreme velocities used in the simulations are labelled as theoretical limits.

Supplementary Note S2: Mesh statistics

Table S1 summarizes the mesh used for each configuration. Because the 2 m × 3 m blankets are discretized with a physics-controlled "extremely coarse" mesh, the element count and the element-size range are reported here for transparency. A full mesh-convergence study at this scale exceeds our computing resources (see the Limitations paragraph in the main text), so the reported values should be read as trend-level estimates rather than mesh-converged predictions.

Table S1. Mesh statistics for the three configurations.

Configuration	Domain size	Mesh setting	Number of elements	Element quality range	Notes
Water-cooled blanket	2 m × 3 m	Physics-controlled, coarse	95500	0.0854~0.458	No local refinement at TE interfaces / flow channels; no

Configuration	Domain size	Mesh setting	Number of elements	Element quality range	Notes
					mesh convergence study
Air-cooled blanket	2 m × 3 m	Physics-controlled, extremely coarse	42081	0.231~1.65	No local refinement at TE interfaces / flow channels; no mesh convergence study
Membrane-cooled blanket	0.2 m × 0.2 m	Physics-controlled, extremely coarse	62627	0.56~3	Thin membrane not locally resolved; no mesh convergence study

Supplementary Note S3: Sensitivity to membrane thermal conductivity

The membrane thermal conductivity was varied from 2 to 1000 $W \cdot m^{-1} \cdot K^{-1}$ with the other properties held fixed. Both the surface temperature difference and the surface heat-exchange power improve with conductivity and saturate above 500 $W \cdot m^{-1} \cdot K^{-1}$. Membrane thickness and interfacial thermal resistance were not varied, and this is stated as a limitation, because anisotropy and interfacial resistance can also influence lateral heat spreading.

Supplementary Note S4: Temperature measurement, calibration and uncertainty

K-type thermocouples (accuracy ±0.5 K) were placed at the surface of the blanket. The infrared camera (NETD < 2 K, 32 × 24 pixels) was operated with an emissivity setting of ε =0.75, calibrated against the thermocouple readings at ambient temperature. Repeat measurements (n = 5) gave a surface-temperature repeatability of ± 1.0 K. The quoted NETD is a noise-equivalent temperature difference, not an absolute accuracy; a complete uncertainty budget including emissivity correction and spatial-averaging effects is not available for this dataset.

Supplementary Note S5: Scaling assumptions for the meter-scale projections

The meter-scale values given for the membrane-cooled architecture are projections obtained under four stated assumptions: (i) a constant module density of 100 modules per m^2; (ii) a constant per-module driving current of 2 A; (iii) a negligible change in per-module thermal resistance with scale; and (iv) linear scaling of the total electrical power and system mass with the regulated area. Under these assumptions, extending the membrane-cooled unit from 0.04 m^2 to 6 m^2 requires about 600 modules and a total electrical input of about 5.27 kW. These are order-of-magnitude estimates, not experimentally validated values.

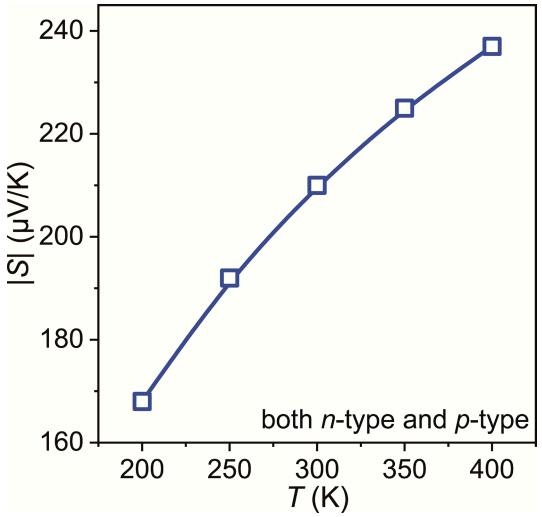

Figure S1 Temperature dependence of |α| for both *n*-type and *p*-type materials in 12706-type thermoelectric cooler.

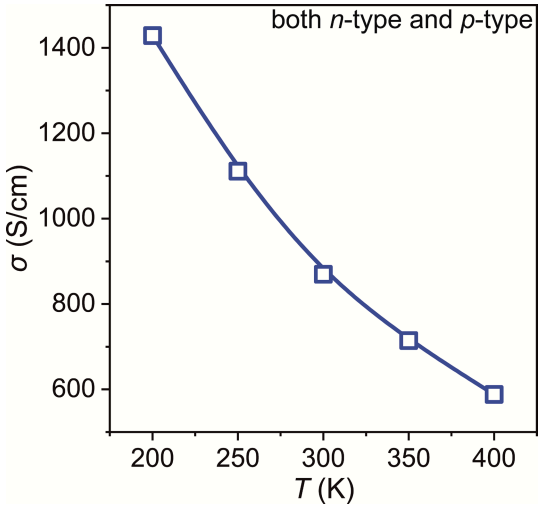

Figure S2 Temperature dependence of σ for both *n*-type and *p*-type materials in 12706-type thermoelectric cooler.

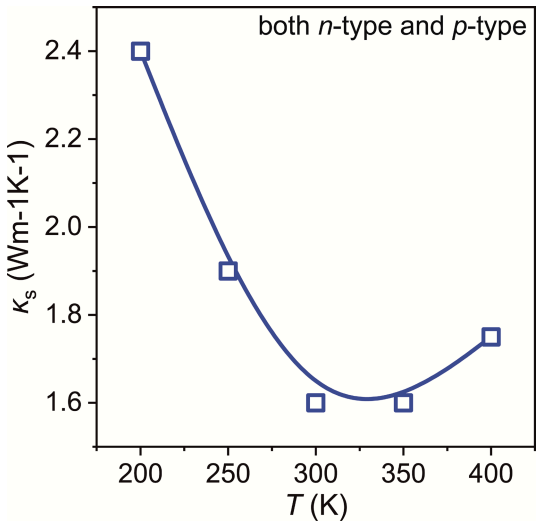

Figure S**3** Temperature dependence of κ_s for both n-type and p-type materials in 12706-type thermoelectric cooler.

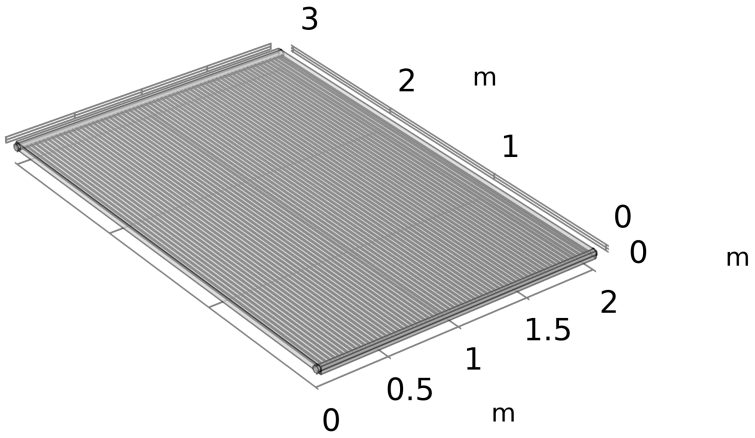

Figure S4 Structural model of the water-cooled blanket.

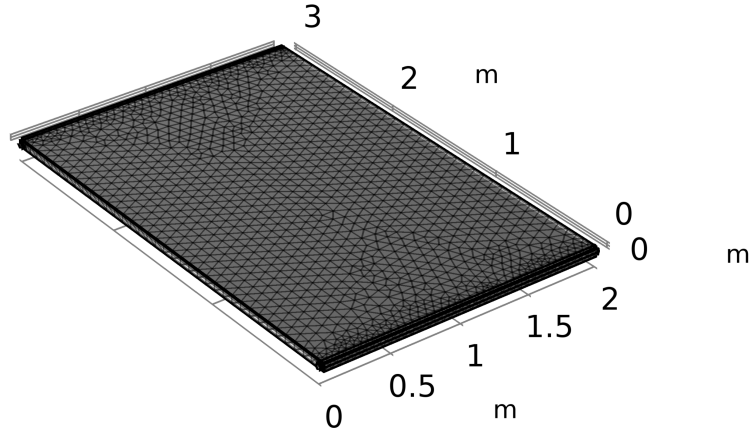

Figure S5 Finite element mesh generation for the structural model of the water-cooled Blanket.

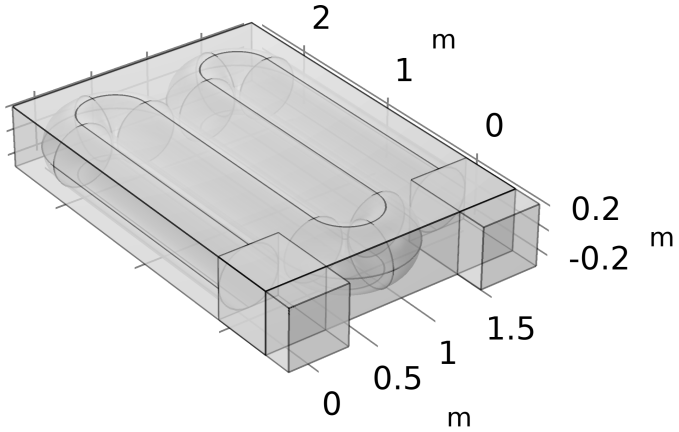

Figure S6 Structural model of the air-cooled blanket.

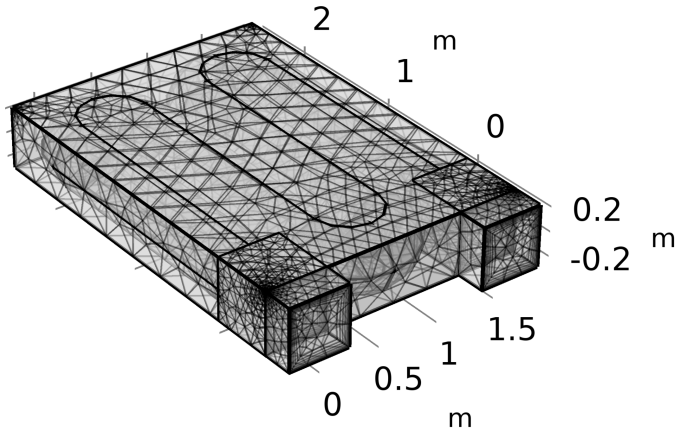

Figure S7 Finite element mesh generation for the structural model of the air-cooled blanket.

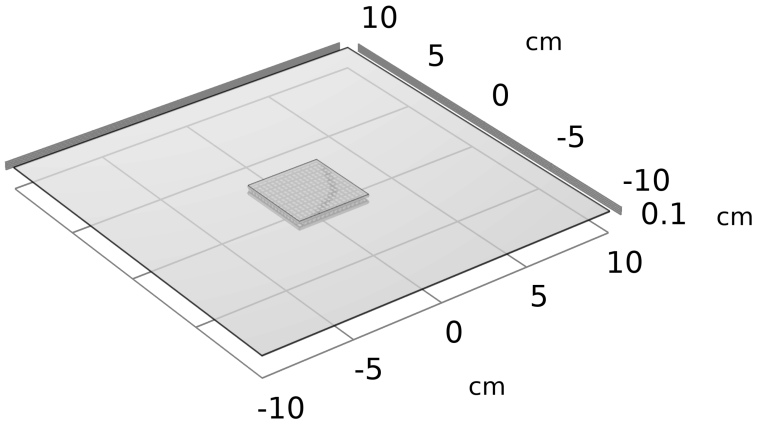

Figure S8 Structural model of the membrane-cooled blanket.

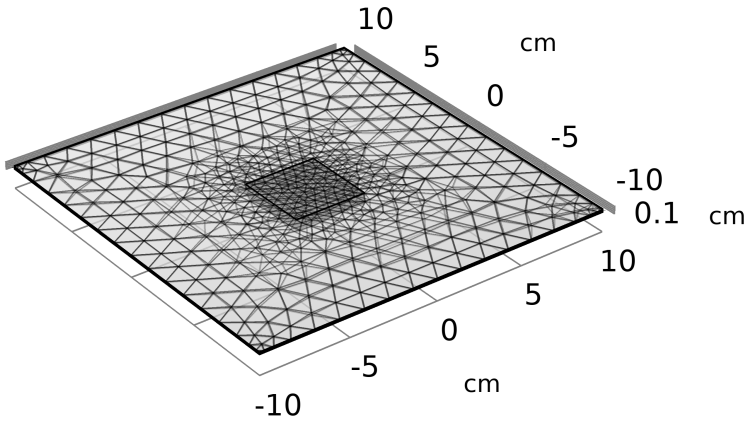

Figure S9 Finite element mesh generation for the structural model of the membrane-cooled blanket.

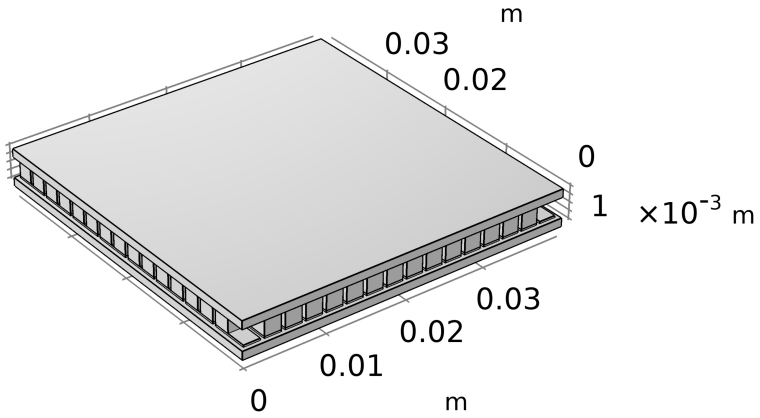

Figure S10 Structural model of the 12706-type thermoelectric cooler.

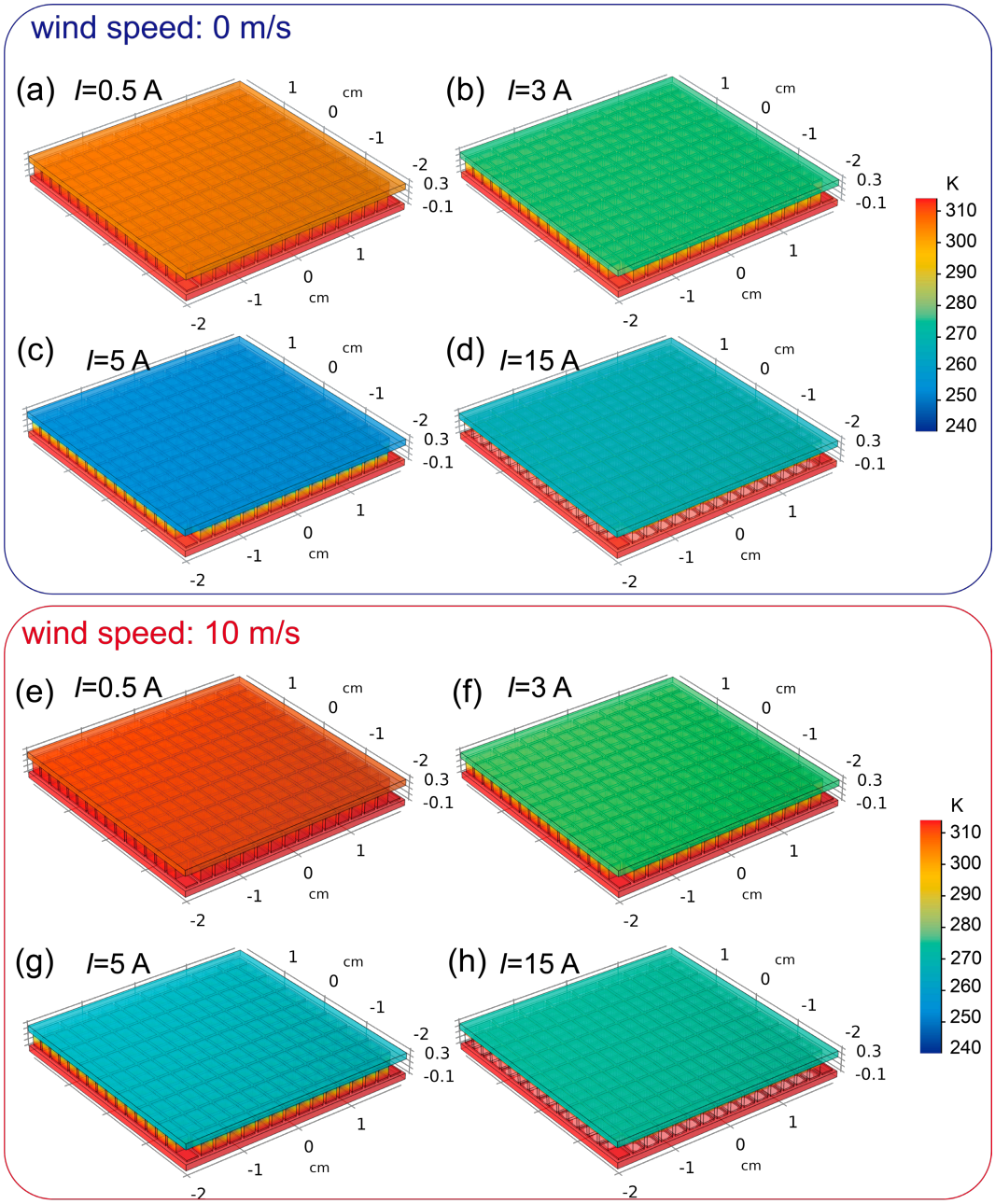

Figure S**11** 3D contour plots of surface temperature for the 12706-type thermoelectric device under varying current and wind speed: (a–d) wind speed 0 m/s; (e–h) wind speed 10 m/s; (a, e) I = 0.5 A; (b, f) I = 3 A; (c, g) I = 5 A; (d, h) I = 15 A.

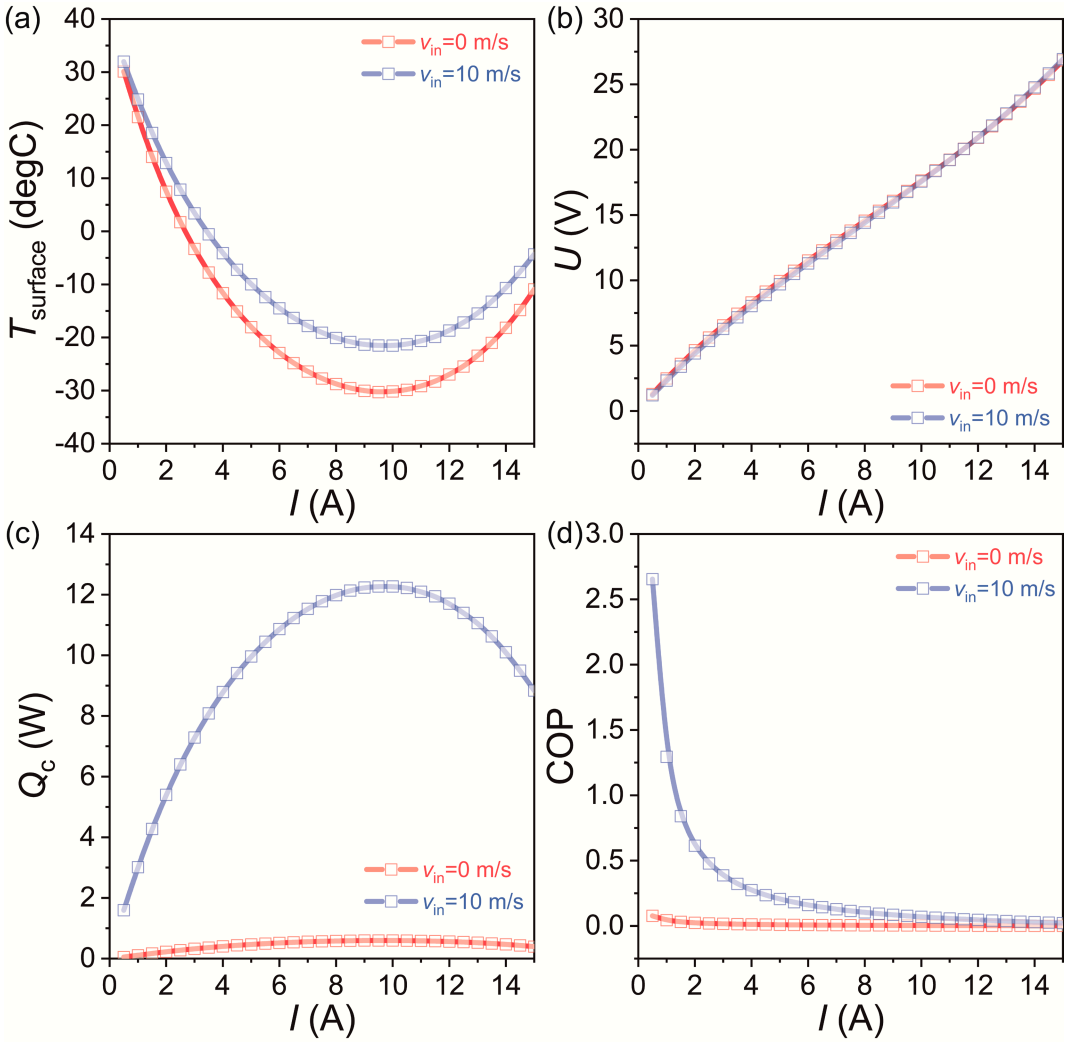

Figure S**12** Current dependence of the thermoelectric device performance under different wind speeds: (a) surface temperature; (b) input voltage; (c) cooling power (Q_c); (d) coefficient of performance (COP).

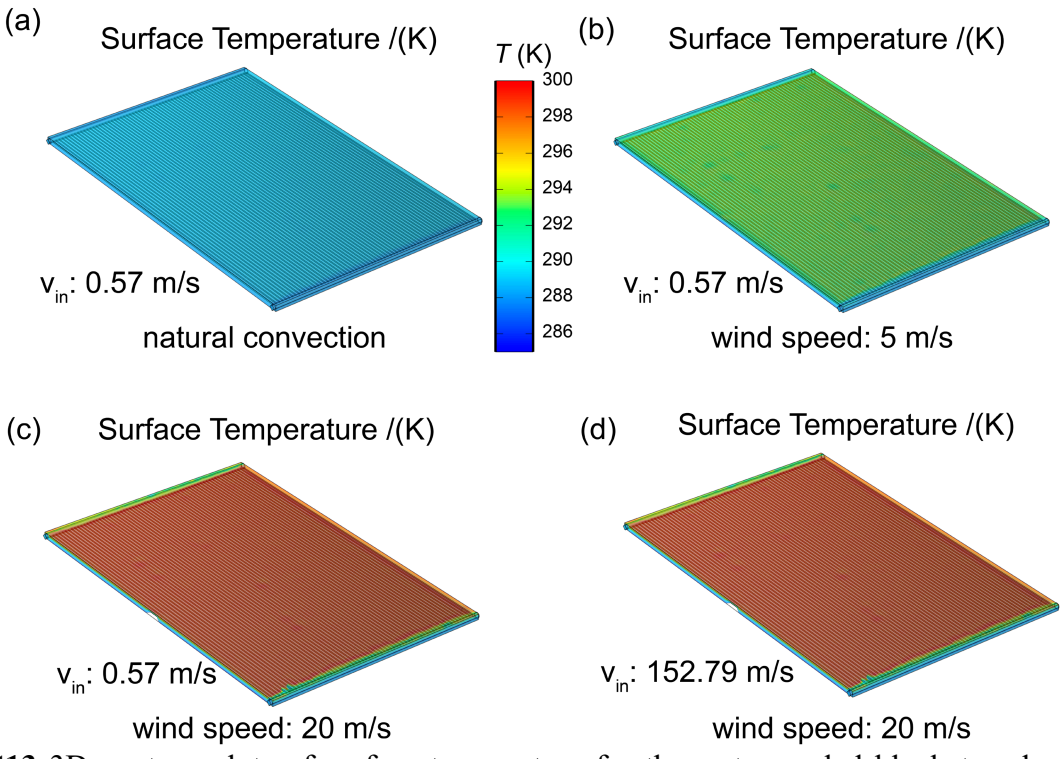

Figure S**13** 3D contour plots of surface temperature for the water-cooled blanket under different conditions: (a) natural convection; (b) wind speed 5 m/s; (c) wind speed 20 m/s; (d) wind speed 20

m/s with a water flow velocity of 152.79 m/s.

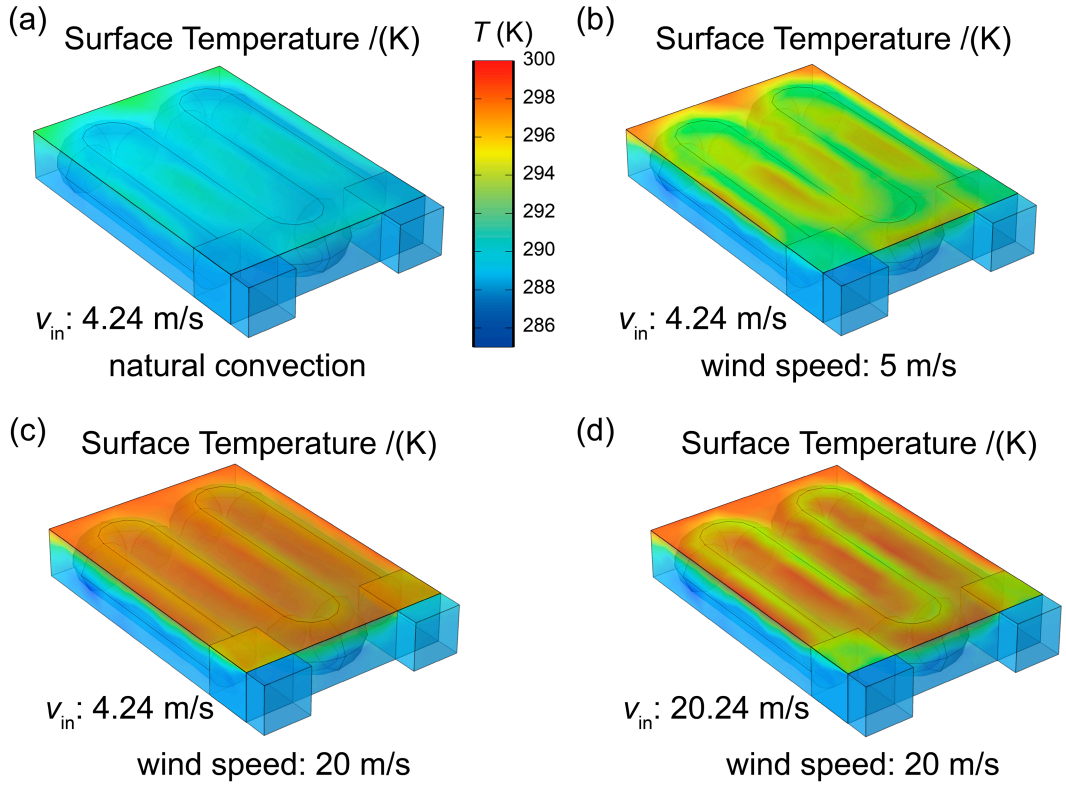

Figure S**14** 3D contour plots of surface temperature for the air-cooled blanket under different conditions: (a) natural convection; (b) wind speed 5 m/s; (c) wind speed 20 m/s; (d) wind speed 20 m/s with an airflow velocity of 20.24 m/s.

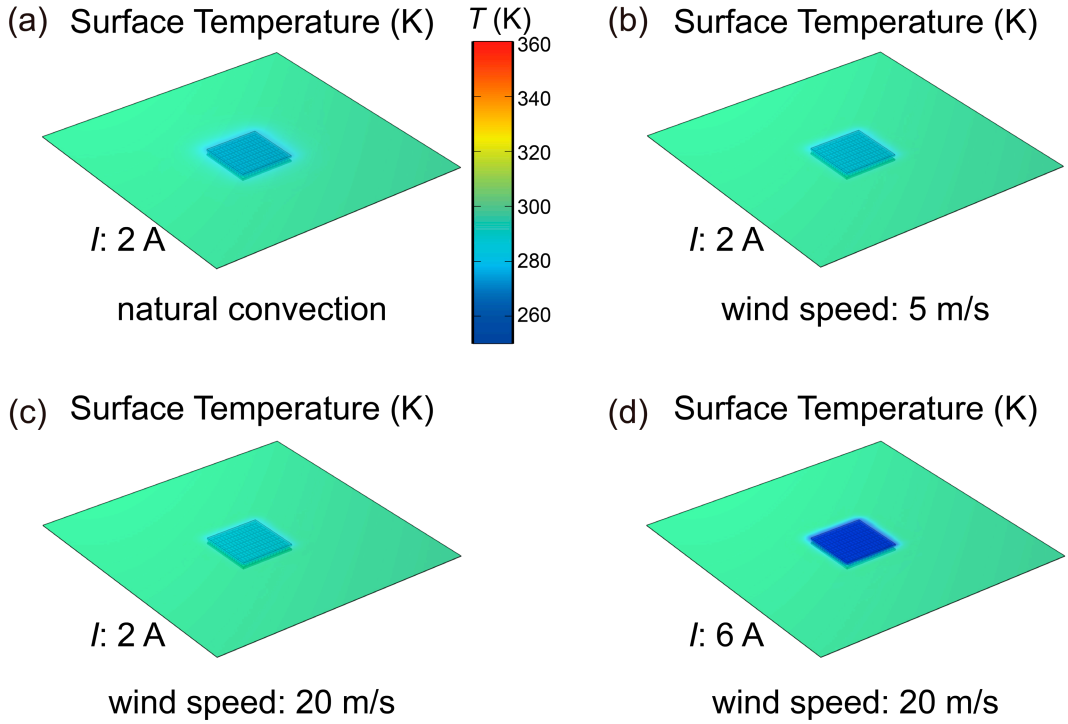

Figure S15 3D contour plots of surface temperature for the membrane-cooled blanket under different conditions: (a) natural convection; (b) wind speed 5 m/s; (c) wind speed 20 m/s; (d) wind

speed 20 m/s with a current of 6 A through the thermoelectric device. The thermal conductivity (κ) of the membrane is set to a deliberately low value of 2 W·m-1·K-1 to illustrate the effect of insufficient lateral heat spreading.

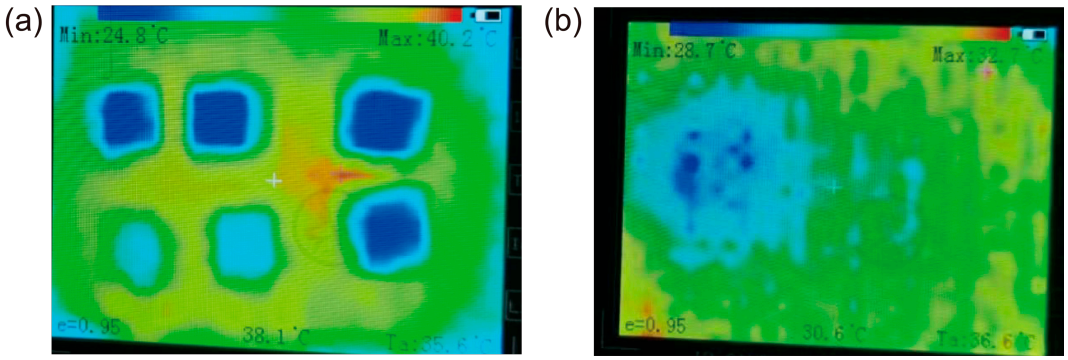

Figure S16 Infrared image of the thermoelectric module with (a) and without (b) a heat-spreading membrane.

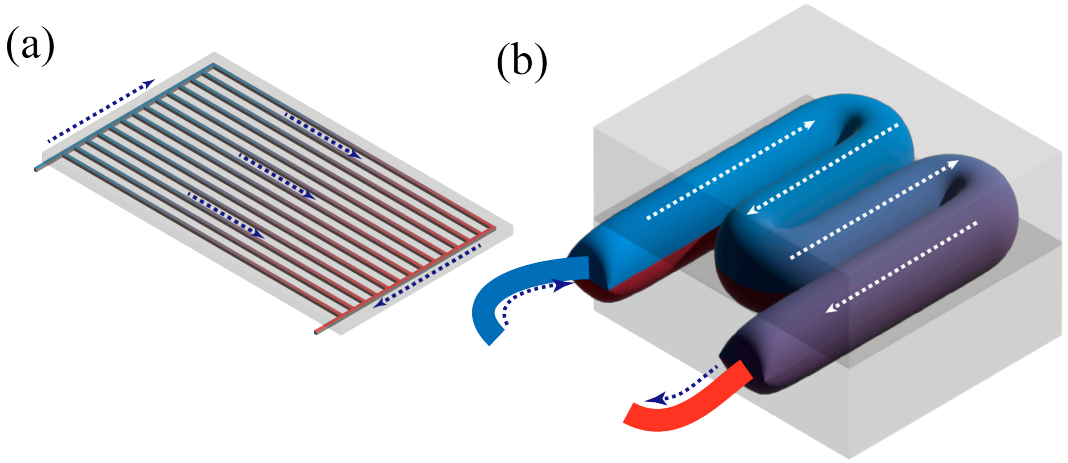

Figure S17 Schematic diagram of fluid flow directions for the two blankets. (A) water-cooled blanket; (B) Air-cooled blanket.